Supporting Online Material for

Enzyme-Free Nucleic Acid Logic Circuits

Georg Seelig, David Soloveichik, David Yu Zhang, Erik Winfree*

*To whom correspondence should be addressed. E-mail: winfree@caltech.edu

Published 8 December, *Science* **314**, 1585 (2006)
DOI: 10.1126/science.1132493

This PDF file includes:

Enzyme-free Nucleic Acid Logic Circuits

(supplementary information)

Georg Seelig,[1] David Soloveichik,[1] David Yu Zhang,[1] and Erik Winfree[1]

[1] *California Institute of Technology, MC 136-93, 1200 E. California Blvd., Pasadena, CA 91125*

MATERIALS AND METHODS

System Specifications. For microRNA translator gates, the length of the gate strand recognition region is determined by the length of the microRNA input and ranges from 20 to 22 nucleotides (*nt*). Toe-holds for input binding are six *nt* long. The recognition region of the output strand is 36 *nt* long of which 27 *nt* are single-stranded before output release. The double-stranded 9 base-pair (*bp*) part of the recognition region includes the toe-hold binding sequence (6 *nt*) and a protecting three *bp* clamp. In all other gates, recognition regions for both input and output strands are 36 *nt* long. The first gate strand in any AND gate as well as the gate strands in gates HI, $Q_{out}P_f$, and WY thus are 36 *mers*. Additional gates strands are 60 *mers*. Output strands are 57 *mers*. Before release, output strands are bound to their gate with both ends. The two binding regions are 15 *bp* long while the single stranded loop region has length 27 *nt*. For design details, see Fig. S1.

DNA oligos were synthesized and purified by Integrated DNA Technologies, Coralville, IA. DNA stock solutions were prepared at a concentration of 50 μM in ultra pure water (purified by a Milli-Q system, Millipore, Bedford, MA). Concentrations were determined from the measured absorbance at 260 nM and the calculated extinction coefficient (calculation based on the nearest-neighbor model with parameters of Ref. [S1]).

RNA oligos with sequences identical to biological microRNAs miR-124a and let-7c were also synthesized and purified by IDT. Mouse brain total RNA samples were obtained from Ambion, Inc., Austin, TX. In Fig. 2A, the concentration of total RNA $\approx 200\mu g/ml$. For comparison, a concentration of 60 nM for input strands corresponds to about 0.6 $\mu g/ml$ RNA. DNA in gate complexes is at $2\mu g/ml$. Total RNA samples mainly consist of ribosomal 18S and 28S RNA. The concentration of gates and added RNA inputs are several orders of magnitude higher than the concentration of any microRNA contained in the total RNA samples. Thus, additional input amplification circuitry would be required to detect endogenous miR-124a and let-7c.

Dye labels were used to follow reaction kinetics: Carboxytetramethylrhodamine (TAMRA) was used as a fluorophore and Iowa Black RQ as a dark quencher. Even though the same fluorophore was used in all our experiments and all dye-labeled strands were ordered HPLC purified, fluorescence intensity was observed to vary strongly between strands with different sequences and between different batches of the same strand.

TAE/Mg^{++} buffer (0.04 M Tris Acetate, 1 mM EDTA, 12.5 mM Mg Acetate, pH 8.3) was used for all reactions including fluorescence experiments, formation gels and gel elutions for purification.

Gel Electrophoresis. Non-denaturing polyacrylamide gels (acrylamide-bis 19:1, 8% or 10%, 2-3 h at 15 V/cm, and 4°C) were used to verify structure formation and to analyze reaction mixtures. For imaging, gels were stained with SybrGold (Molecular Probes, Eugene, OR) for 25 to 35 min, excited at 488 nm and imaged with 530 bandpass filter on a Bio-Rad (Hercules, CA) Molecular Imager FX Pro Plus.

Gate Formation and Purification. Gates were formed in a slow anneal where the reaction mixture is heated up to 90°C and then slowly (1°C/min) cooled down to room temperature. Each gate sample was formed in a separate reaction.

For purification, gates were prepared at 10 or 20 μM. In our initial experiments gates were purified from a gel directly after annealing. Gel elution (4-5 h at 5 V/cm and 4°C) was done using the Elutrap Electroelution System (Schleicher and Schuell Biosience, Dassel, Germany). Purification allowed for the separation of fully from partially assembled structures and dramatically decreased leak signals due to false triggering in fluorescence experiments. However, false triggering could not be completely eliminated with this approach, probably because gates with only minor defects (e.g. gates containing incorrectly synthesized strands with only a few bases missing) co-migrate with the error-free gates in the gel.

In order to at least partially eliminate gates with minor defects, an improved purification scheme was developed. In this approach, gates were incubated with their inputs overnight at room temperature before purification. Importantly, first-acting inputs were truncated such that they would not react with correctly formed gates. Specifically, toe-hold binding regions were removed from inputs targeting gate strands with a single stranded toe-hold, i.e. the first input in an AND gate and inputs to translator gates. (For translator gates taking microRNA input, in addition to truncating the toe-hold, the strand was extended by 3 *nt* to cover the 3 *nt* clamp shown in Fig. S1.) Second and third inputs to

AND gates need not be truncated: in fully assembled gates, all regions that could potentially bind them are double stranded. Correctly formed gates assembled from full length strands should not react with these inputs. However, malformed gates or gates containing strands with synthesis errors can potentially react with these inputs. Inputs were added at substoichiometric concentrations between 5 or 10 μM per input. After incubation, purification proceeded as described above. Incubation with inputs suppressed leak signal further, in some cases to undetectable levels. Comparison of purified and unpurified gates is shown in Fig. S3. Purification of the catalytic gates is as described in Ref. [S2].

After purification, the effective concentrations of the gates were estimated from a measurement of the absorbance at 260 nm and the calculated extinction coefficients for the gates. The extinction coefficient for a gate was approximated by the sum of the extinction coefficients of its constituent segments (loops, toe-holds, double-stranded sections or dye-labels). Extinction coefficients were calculated independently for all the single stranded (e.g. toe-hold and loop-regions) and double stranded segments. The extinction coefficients e_{ds} for the double stranded sections were calculated using the phenomenological expression $e_{ds} = e_{ss}(seq) + e_{ss}(\overline{seq}) - 3200 \times N_{AT} - 2000 \times N_{GC}$. Here $e_{ss}(seq)$ is the the extinction coefficient of one component strand in the duplex in its single stranded state, $e_{ss}(\overline{seq})$ is the same for complementary sequence in the duplex and N_{AT} and N_{GC}, respectively, are the number of AT- and GC-pairs in the duplex. The magnitude (per base pair) of the negative correction to the extinction coefficient of a duplex was estimated from Fig. (1) in Ref. [S1]. The extinction coefficients for fluorophore and quencher provided by IDT were used (TAMRA: $e = 29100$, Iowa Black RQ: $e = 50457$).

Kinetics Measurements and Fluorescence Data Normalization. The experiments for Fig. 2A of the paper were performed on a SPEX Fluorolog-3 (Jobin Yvon Horiba, Edison, NJ), with excitation at 559 nm (2 nm bandwidth) and emission at 583 nm (10 nm bandwidth), recorded every 30 seconds. All other kinetics experiments were done in a fluorimeter custom built by Bernard Yurke. The fluorophores were excited at 532 nm and emitted fluorescence intensity was integrated from 550 nm to 600 nm. Fluorescence experiments were performed with each reaction volume of 100 μl maintained at 25°C (37° for Fig. 2A) and reactant concentrations ranging from 10 nM to 1 μM. Gates were mixed in a test-tube before the start of each experiment with one dye/quencher-labeled gate serving as a read-out.

In a typical experiment, four samples were run in parallel and one data point (per sample) was acquired every second. Of the four instrument channels available, one was used for measuring a reference sample and only three were used for kinetics experiments. The reference sample contained a single dye-labeled strand of DNA and was prepared afresh at least every two days (to compensate for photo bleaching and sample loss due to evaporation). The signal strength of the reference sample should remain constant in the absence of noise, so measuring a reference allowed monitoring fluctuations in laser intensity and other sources of (channel-independent) instrument noise.

The four instrument channels were not completely identical and the signal strength varied between the four channels. Differences were either due to uneven splitting of the exciting laser light between the four samples, scattering effects along different optical paths or, due to variations in amplification or detection efficiencies between photo-diode detectors. These channel-to-channel variations were maximally on the order of 35 % and were found to be constant on time-scales relevant for our experiments.

The raw experimental data was corrected for these channel-to channel variations as follows: At the end of each experimental run, all four samples (including the reference) were removed and then, in turn, moved to the same instrument channel where the signal was recorded for 1-5 minutes. In addition, the cuvette containing the reference sample was moved to the three slots used for kinetics experiments and the signal strength was recorded for 1-5 min. Either set of measurements allowed subsequent adjustment of the raw data for channel-to-channel variations, and both methods gave equivalent results.

The amount of instrument noise varied between experiments. For most of the data shown in this paper, noise did not not exceed 1% of the signal. However, noise up to 10 % of the signal was not unusual. In situations where noise was clearly correlated between all four channels (most probably noise to to laser intensity fluctuations), experimental data was divided by the reference signal in order to correct for this noise.

Initial fluorescence was measured for at least one hour before inputs were added, in order to determine the fluorescence base-line and also to make sure that the read-out gate was not triggered spontaneously due to spurious interactions with other gates in solution. Initial fluorescence due to incomplete quenching was typically on the order of or less than 5 % of the final signal. However, on rare occasions, the initial signal could be as high as 15-20 % of the final signal. In cases where the read-out gate was not fully triggered at the end of an experimental run (e.g. because of slow kinetics) the read-out gate was triggered explicitly by addition of extra inputs and the final value was recorded. Data was subsequently normalized such that the signal measured before addition of inputs corresponded to zero while the signal of the fully triggered read-out gate corresponded to one.

Finally, for presentation in the paper all data was shifted such that the time of input addition corresponds to time $t = 1$ hour in order to make comparison of the reaction kinetics between different fluorescence traces easier.

Sequence design. Except where constrained by biological sequences or pre-existing DNA devices, all sequences were design by computer optimization. In the design process, the main structural constraints were imposed from the outset, such as domain lengths and complementarity requirements. In particular, recognition regions of output gate strands must be complementary to their target and each gate strand must be able to correctly bind its neighboring gate strand(s). In some cases, double-helical domains were terminated by G-C pairs to reduce fraying. Input strand sequences were entirely determined by sequence of their target gate strand. Sequences were designed incrementally as the research progressed; in each design stage, strand sequences from the previous stages constrained choices for the new gate sequences.

In each stage, a set of random sequences obeying these structural constraints are then generated and an iterative optimization scheme is applied to them. The optimization process allows one to implement a set of additional soft constraints. These included: (i) minimization of secondary structures in single-stranded species (the input and messenger strands), as predicted by the minimum-free-energy (MFE) structure [S3] at 25°C using DNA parameters [S4]; (ii) minimization of cross-talk between all single-stranded species, as measured by the ΔG° of association between pairs of strands (estimated as intramolecular MFE for a 'virtual' strand linking the two sequences via 5 unpaired nucleotides); (iii) especially avoiding secondary structure in messenger strands and single-stranded portions of partially-triggered gates that hides the toe-hold binding region; (iv) avoiding a set of undesired sequences (e.g. more than three consecutive repeats of the same base); (v) minimizing the occurrence of short subsequences (3 to 10 base pairs) that have exact or near-exact complementary matches elsewhere either in the same strand or in other strands, except as intended by design (generally referred to as sequence symmetry minimization [S5, S6]); (vi) making all toe-holds of similar strength (predicted ΔG° at 25°C); (vii) avoiding branch migration of the bulge loop region in a bound output strand: this is achieved by imposing that the first four single-stranded nucleotides at the base on one side of the loop are different from the last four nucleotides in the double stranded region directly adjacent to the loop on the other side. Scores for each of these soft criteria were weighted and summed to obtain an overall score for the set of sequences being designed. Sequence optimization proceeded by random descent to minimization of the overall score: sequence mutations were made randomly (subject to satisfying the structural constraints) and accepted if the score was reduced. If the final sequences were unsatisfactory, the scoring weights were adjusted, new initial sequences were chosen, and optimization was attempted again.

A set of toe-holds was designed in the first stage, then the $ABCD$ gate was designed, then the WY and PQ gates, then the EFG gate and most translators (including the full translator, but excluding UV and ST), and finally the UV and ST translators (whose microRNA targets were chosen to share a 6 nt toe-hold domain) were designed to demonstrate implicit OR. The catalytic amplifiers CA and R were designed by cutting-and-pasting appropriate recognition domains into the molecules described in Ref. [S2]. Similarly, the sequences for the threshold gate were primarily defined by pre-existing sequences.

Derivation of sigmoidal threshold behavior. If the amount of A_{out} is small, and thus threshold gates remain mostly unreacted, then the probability that a single threshold gate reacts with two molecules of A_{out} is roughly quadratic in the amount of A_{out}. Consequently, in this regime, the relationship between A_{out} and the amount of triggered threshold should be approximately quadratic. If the amount of A_{out} is large and most of the threshold gate has reacted with A_{out} at least once, then there is a linear relationship between A_{out} and the amount of triggered threshold, until A_{out} is greater than twice the amount of threshold where saturation is observed. A simple two equation model is sufficient to approximately explain the resultant sigmoidal transfer function over the entire input range (a single parameter fit matches the data of Figs. 2C and S5D to within $\approx 10\%$):

$$A_{out} + Th \xrightarrow{k_1} Th'$$
$$A_{out} + Th' \xrightarrow{k_2} Th''$$

where Th, Th', and Th" represent three states of the threshold gate, with the last state being triggered. (Including the intermediate reaction with $Th2_{in}$ is necessary for greater physical plausibility but the principle of the operation of the threshold gate can be explained without it.)

A larger threshold gate taking $n > 2$ molecules of A_{out} as input should provide a better than quadratic non-linearity: using the above intuition, the transfer function should be of power n for low amounts of A_{out}.

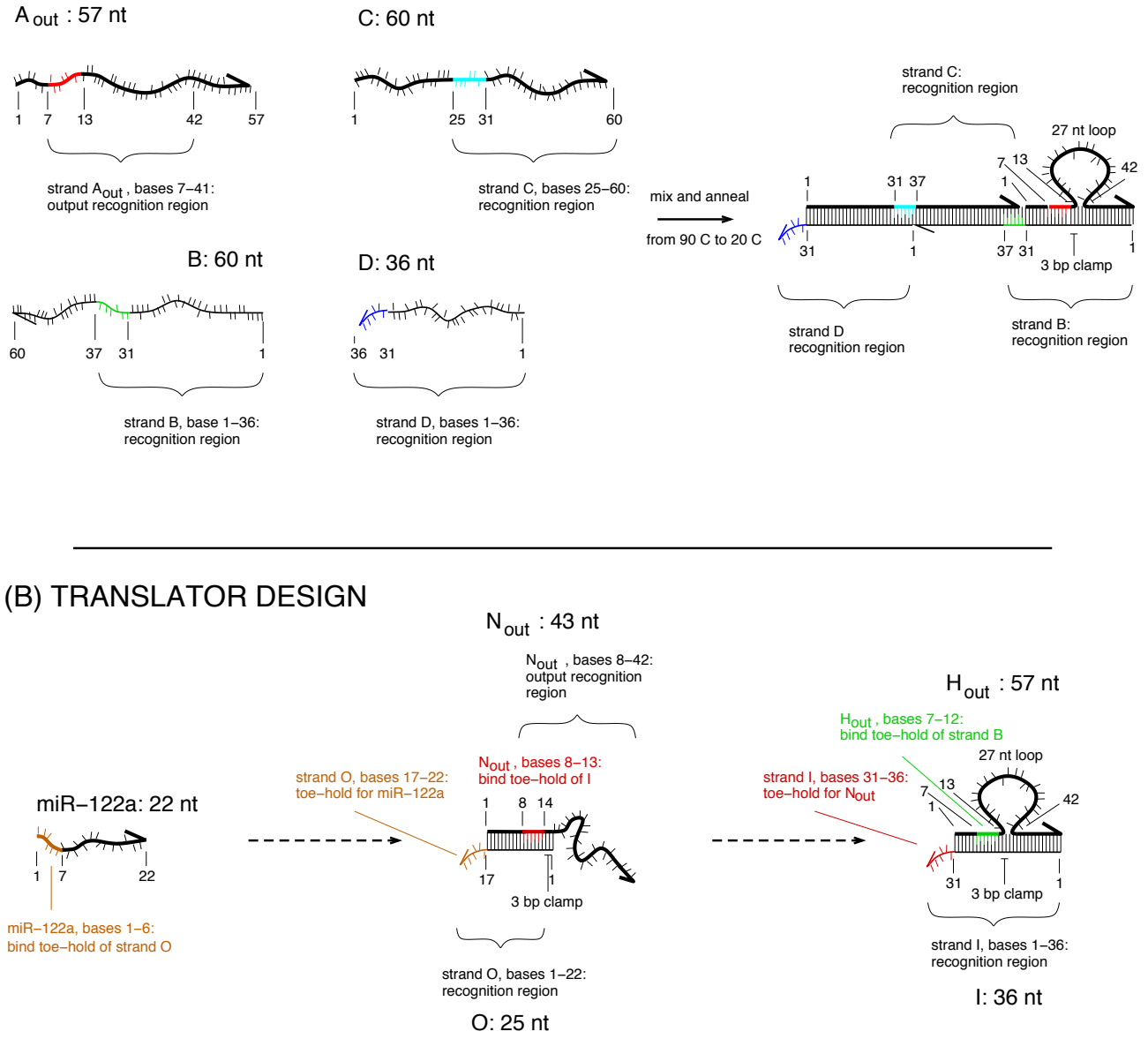

FIG. S1: Gate design. In all figures, solid arrows indicate a chemical reaction, in this case $A_{out} + B + C + D \rightarrow ABCD$. A dashed arrow indicates where an input strand or output strand may bind to a toe-hold in a downstream gate complex and thereby serve as an input to the gate. All toe-hold sequences and toe-hold binding sequences are indicated in color. Sequences of identical color bind to each other. Numbers refer to bases and the first base in every sub-sequence (i.e. region of different color) is indicated. In unbound strands the last base of the strand is also labeled explicitly. **(A)** Gate design and assembly. Constituent strands of a three input AND gate and the final assembled gate are shown. Recognition regions are indicated. If the output strand A_{out} is bound there are three base pairs between the (double-stranded) toe-hold binding sequence (red) and the single-stranded loop. The toe-hold binding region was shifted inward to minimize interactions of a bound output strand with down-stream gates due to spontaneous fraying of the double helix at the nick. This choice implies that a total of nine nucleotides are common to the upstream input and the downstream recognition region. **(B)** Two-stage translator cascade. The length of the recognition region of the first translator is imposed by the length of the microRNA. Only one end of output strand N_{out} is bound to strand O. In order to better protect the toe-hold binding sequence, a three base clamp is introduced. Note that strand O is longer than the input strand miR-122a and that the three nucleotides constituting the clamp remain single stranded when input miR-122a is fully bound. These three bases on strand O in principle provide a toe-hold for the reverse reaction, i.e. N_{out} binds to O and kicks off miR-122a. However, the toe-hold is short and this reaction does not seem to be important. The second translator in the cascade (gate HI) is designed analogously to the gate described in (A).

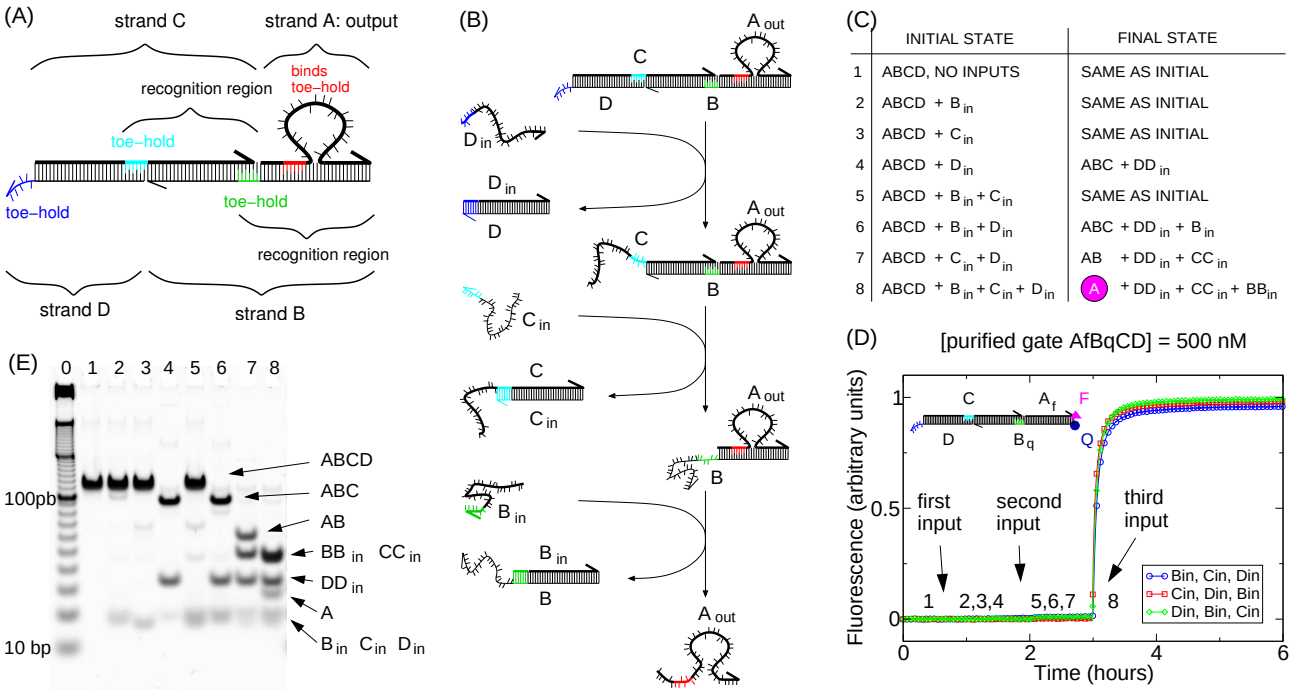

FIG. S2: Schematics of gate operation. (**A**) The gate consists of four DNA strands labeled A (output strand, 57 *mer*), B (60 *mer*), C (60 *mer*) and D (36 *mer*). The 3'-ends of all strands are marked by arrows. Toe-holds and toe-hold binding regions (all 6 *nt*) are indicated in color. (**B**) Calculation of logical AND of three inputs. Input strands B_{in}, C_{in} and D_{in} are 36 *mers* complementary to recognition regions within the corresponding gate strands B, C and D (strand D consists entirely of its recognition region). The calculation proceeds through a series of toe-hold mediated strand displacement reactions. Input strand D_{in} binds at the exposed toe-hold (blue) of strand D and then displaces D from the gate by three-way branch migration. In the process, waste product DD_{in} is formed and a toe-hold for C_{in} (cyan) becomes available. Subsequently, input C_{in} releases strand C forming the CC_{in}-duplex. Then, input B_{in} forms a duplex with strand B and the output strand A_{out} is released into solution. (**C**) Truth table for the three-input AND gate. Only if all three inputs are present the output strand will be released (entry 8). The released output strand is highlighted. (**D**) Fluorescence experiments. For fluorescence experiments, strands A_f (labeled with a fluorophore at the 3'-end, but without the bulge loop) and B_q (quencher at the 5'-end) were used instead of A_{out} and B. The gate used for fluorescence experiments is shown in the inset and fluorophore (F) and quencher (Q) positions are indicated. Fluorescence is quenched initially; an increase in fluorescence is a measure of the progress of the reaction. Inputs are added sequentially with one hour delay between additions. The order of input addition is permuted cyclically between the three fluorescence traces. In this way, all eight entries of the truth table are covered in only three experiments. In the blue trace, for example, we start with the gate and no input (entry 1), then add B_{in} (entry 2), then C_{in} (entry 5) and finally D_{in} (entry 8). The numbers in the figure refer to the entries in the truth table. Experiments are done at 25°C at a concentration of 500 nM for all species. (**E**) Electrophoresis gel. Lane 0: 10 *bp* ladder. Lanes 1-8: The samples are as described in entries 1-8 of the truth table. The gate used in this experiment is as shown in (A), except that for historical reasons strand A rather than A_{out} was used; these strands differ only in the bulge loop sequence.

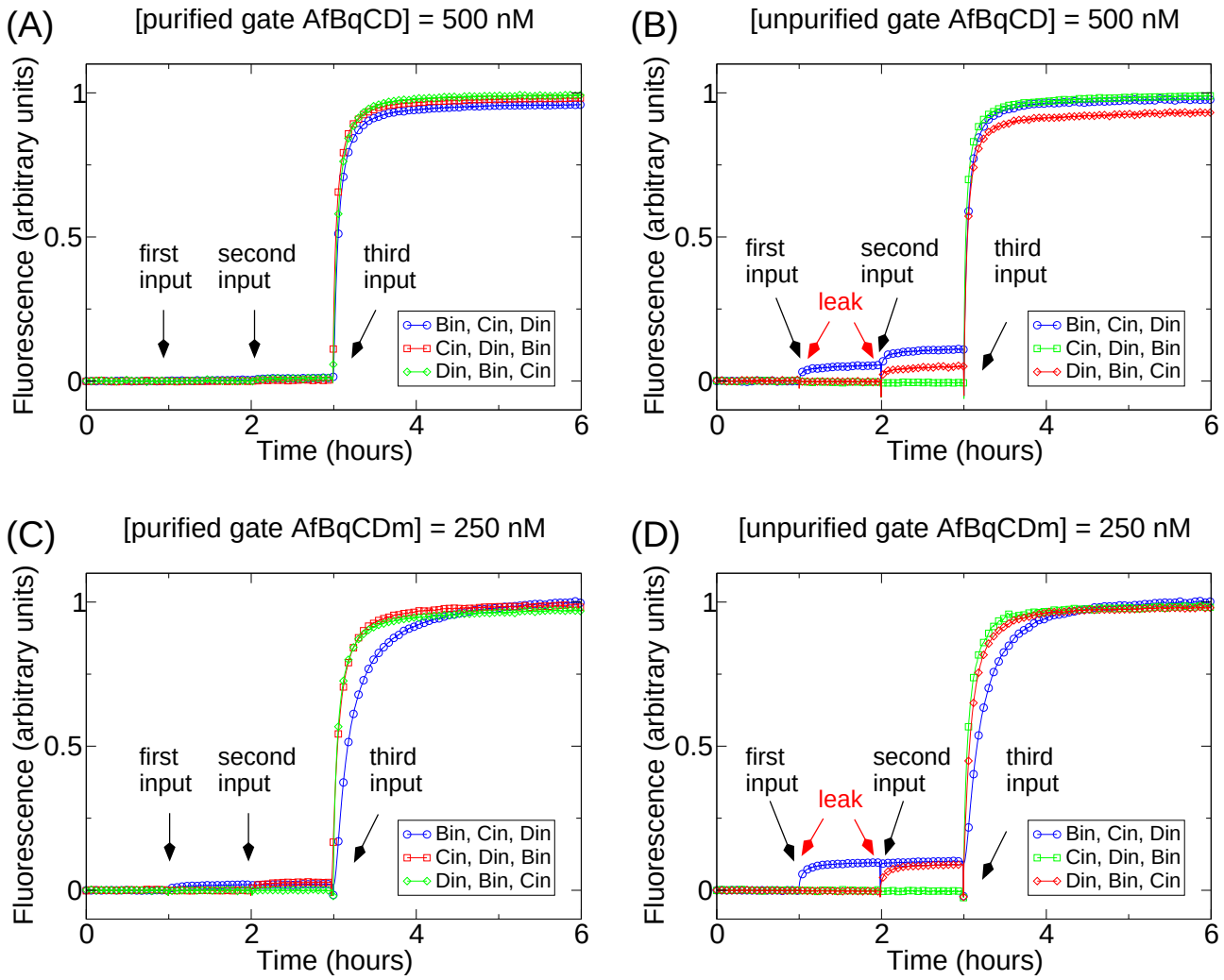

FIG. S3: Three-input AND gate fluorescence data: comparison of purified and unpurified gates. **(A)** Purified AND gate $ABCD$ at 500 nM concentration. **(B)** Unpurified AND gate $ABCD$ at 500 nM concentration. The gates in (A) and (B) were prepared within a few days from each other. The strands used for both gates came from the same DNA stocks. **(C)** Purified AND gate $ABCD_m$ at 250 nM concentration. **(D)** Unpurified AND gate $ABCD_m$ at 250 nM concentration. The gates in (C) and (D) were also prepared within a few days from each other with strands from the same stock solutions. Note that the only difference between strands D and D_m is the sequence of the six nucleotide toe-hold. The gates are otherwise identical. Comparison of (A) and (B) (or (C) and (D)) shows that purification dramatically decreases the amount of false positive signal. For the samples containing unpurified gates (see (B) and (D)) a spurious signal is observed even if only some subset of inputs is present. Also note, that while purification always decreases the leak, the purified samples are not always equally pure. Clearly, the sample used for (C) seems to be more leaky than the one use for (A).

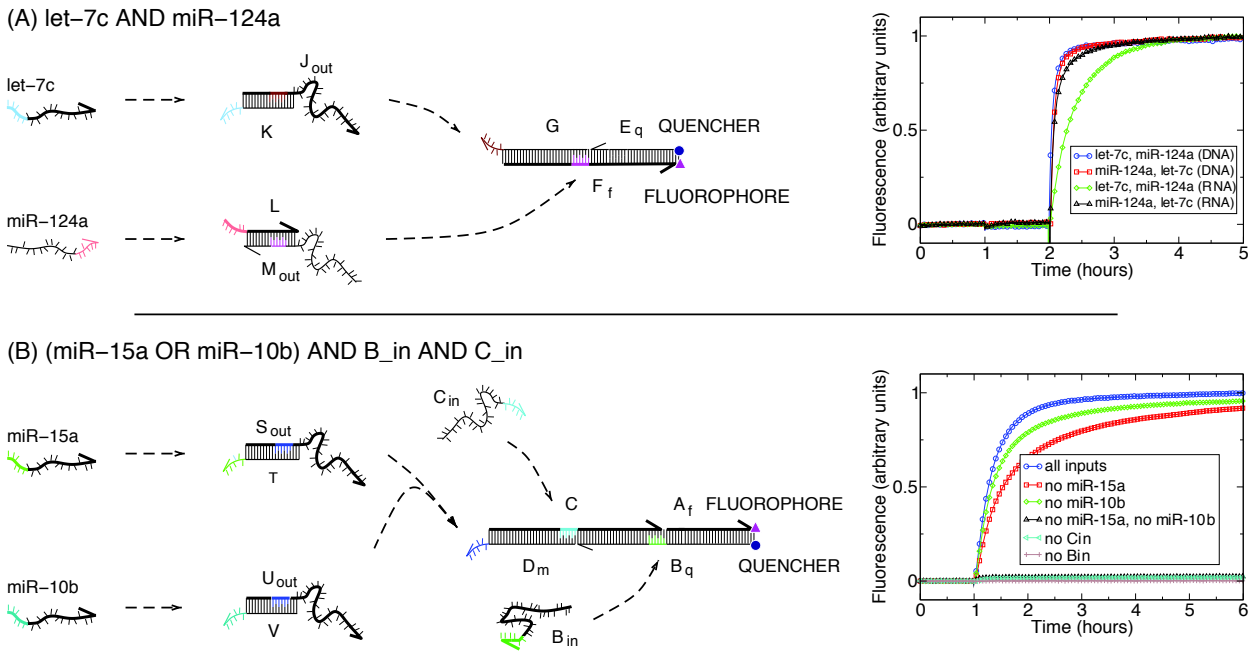

FIG. S4: (**A**) Logical AND: Comparison of reaction kinetics with DNA and RNA inputs. Gate concentration is 250 nM and input concentration is 300 nM. Reactions were carried out at 25 °C in the absence of total RNA. Blue and red trace: DNA inputs. The order of input addition is interchanged between the two traces. In this way, all four cases of the truth table (i.e. no inputs, only miR-124a, only let-7c, both inputs) can be tested in only two experiments. Green and black trace: RNA inputs. The kinetics seem to be a little bit slower with RNA inputs (even though RNA-DNA binding is assumed to be stronger than DNA-DNA binding) but nevertheless the gates operate reliably. (**B**) Implicit OR. Gate concentration is 250 nM and input concentration is 300 nM. Experiments were performed at 25 °C here and in all following experiments. DNA equivalents of the biological microRNAs are used. As expected, the output is triggered only if at least one of miR-15a or miR-10b is present together with B_{in} and C_{in} (blue, red, and green traces).

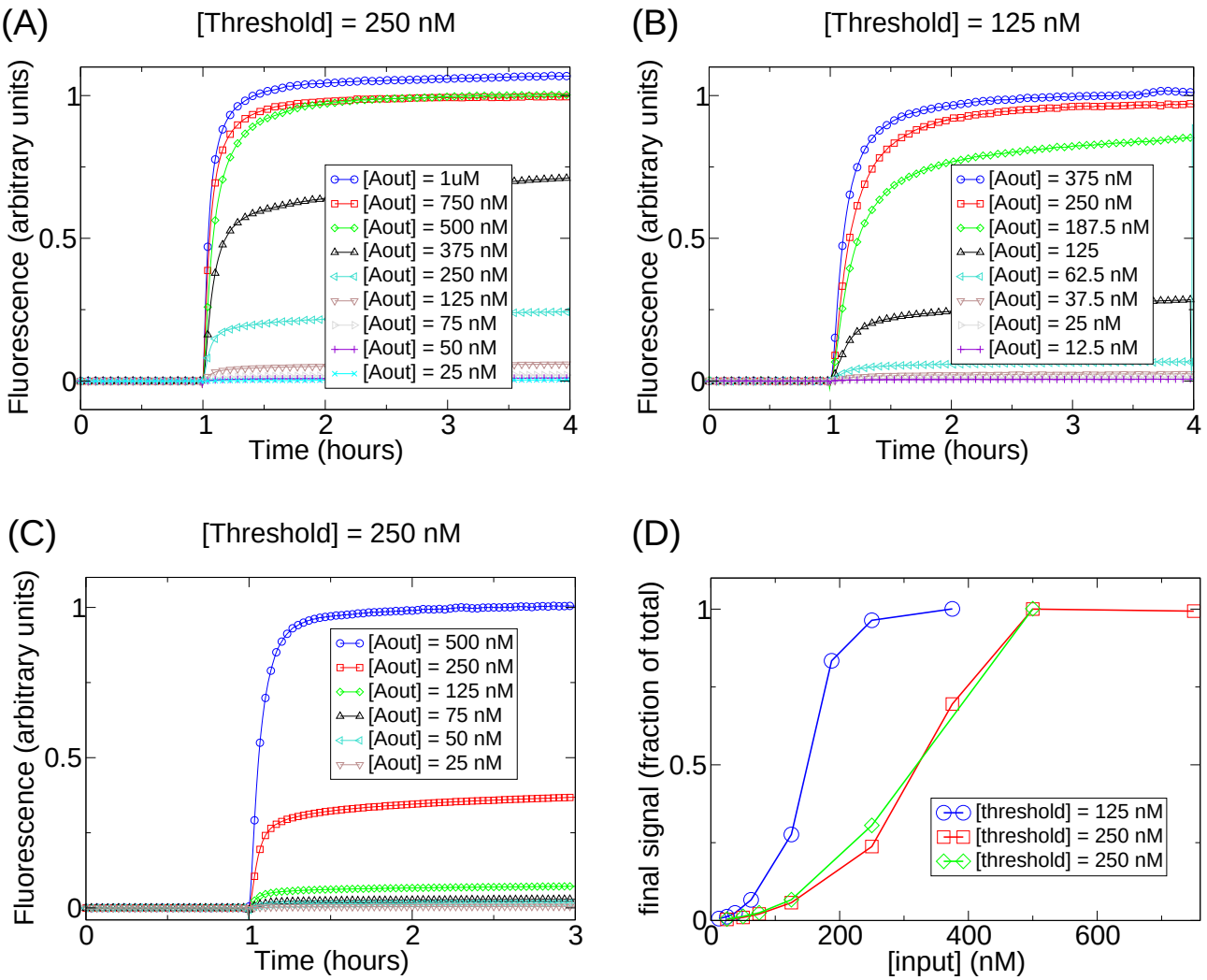

FIG. S5: Fluorescence data for the threshold circuit of Fig. 2C in the paper. All three data sets (see (A), (B) and (C)) are normalized to the maximal signal reached within the respective set of experiments. **(A)** Threshold gate and readout gate at 250 nM, $Th2_{in}$ at 300 nM and varying input concentrations. **(B)** Threshold and readout gate at 125 nM, $Th2_{in}$ at 150 nM and varying input concentrations. **(C)** Same as (A) but with gates from a different purification run. **(D)** Each data point corresponds to the final (normalized) fluorescence value reached in one kinetics experiment. Final fluorescence values are plotted against input concentration. Blue and red curve are the same as in Fig. 2C. The blue curve is obtained from the data shown in (B), the red curve is obtained from the data in (A) and the green curve form the data in (C). Comparison of the red and green curves shows that thresholding behavior can be reproduced with gates from different purifications.

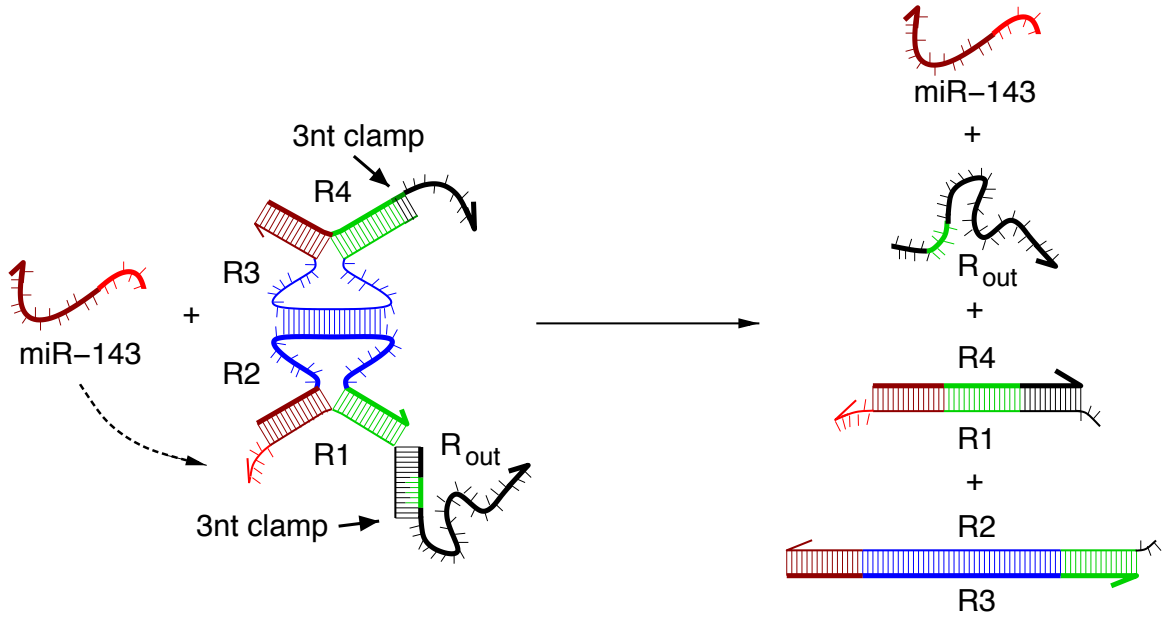

FIG. S6: Input amplifier based on the hybridization catalyst of Ref. [S2]. The 3'-end of each strand is indicated by an arrow. Toe-holds are indicated in color and thin and thick line segments of the same color are complementary to each other. Three base pair clamps introduced for increased stability of the amplifier are indicated. The amplifier complex is trapped in a metastable configuration in which not all possible base pairs are formed. Binding of the input strand opens up one arm of the amplifier complex. This binding event leads to a conformational rearrangement and the amplifier complex decays into two double stranded waste products, the minimum energy state. In the process the output strand is released and, importantly, the input is also released. The input strand is thus available to interact with another amplifier.

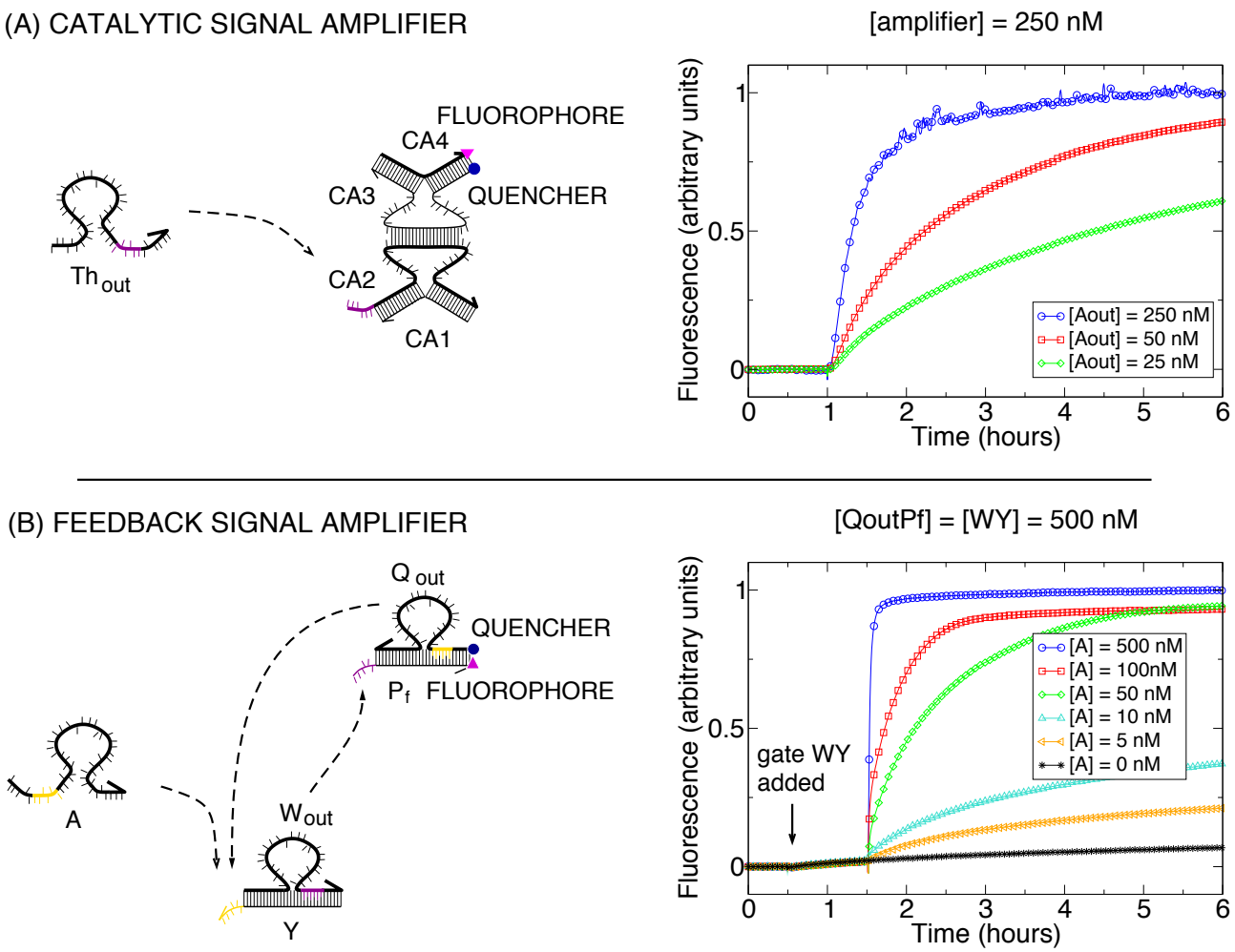

FIG. S7: Signal amplification circuits. **(A)** Signal amplifier based on the hybridization catalyst of Ref. [S2]. The amplifier gate is at 250 nM concentration. The sequences were changed relative to the original hybridization catalyst such that strand Th_{out} can be used as an input. With the original sequences, reaction half-times in a single turnover situation at 250 nM were on the order of 5-10 minutes and in a multiple turnover situation a single catalyst strand (input) could catalyze the decay of up to 40 amplifier gates (there called "fuel complexes"). Here the reaction halftime is on the order of 20-30 minutes and a single strand turns over only about ten amplifier molecules. Note that the input used here (strand Th_{out}) is considerably longer than the input (catalyst strand) of Ref. [S2] and secondary structure effects may slow down binding to the amplifier. **(B)** Amplifier based on feedback. Here, a two-gate feedback circuit amplifies the fluorescence output signal without producing an output messenger strand. It consists of two translators such that the output of the first acts as an input for the second and the output of the second acts as input for the first. This fluorescence amplifier amplifies the output signal linearly with time. Both gates are at 500 nM concentration. In these experiments, strand A (input to gate WY) was used to initiate the feedback loop. When the amplifier is used in the context of a circuit, strand Th_{out} will serve as input. Note that Th_{out} is an input to the dye-labeled gate $Q_{out}P_f$ and $Q_{out}P_f$ can thus be used by itself as a readout gate. For testing of the amplifier, strand A is a better choice since both gates need to be triggered before a signal increase is observed. Half-times in a single turnover situation (at 500 nM) are on the order of 5 min. The feedback system is less stable than the catalytic amplifier in the absence of input. Some spontaneous triggering can be clearly observed when gate WY is added to a solution containing $Q_{out}P_f$.

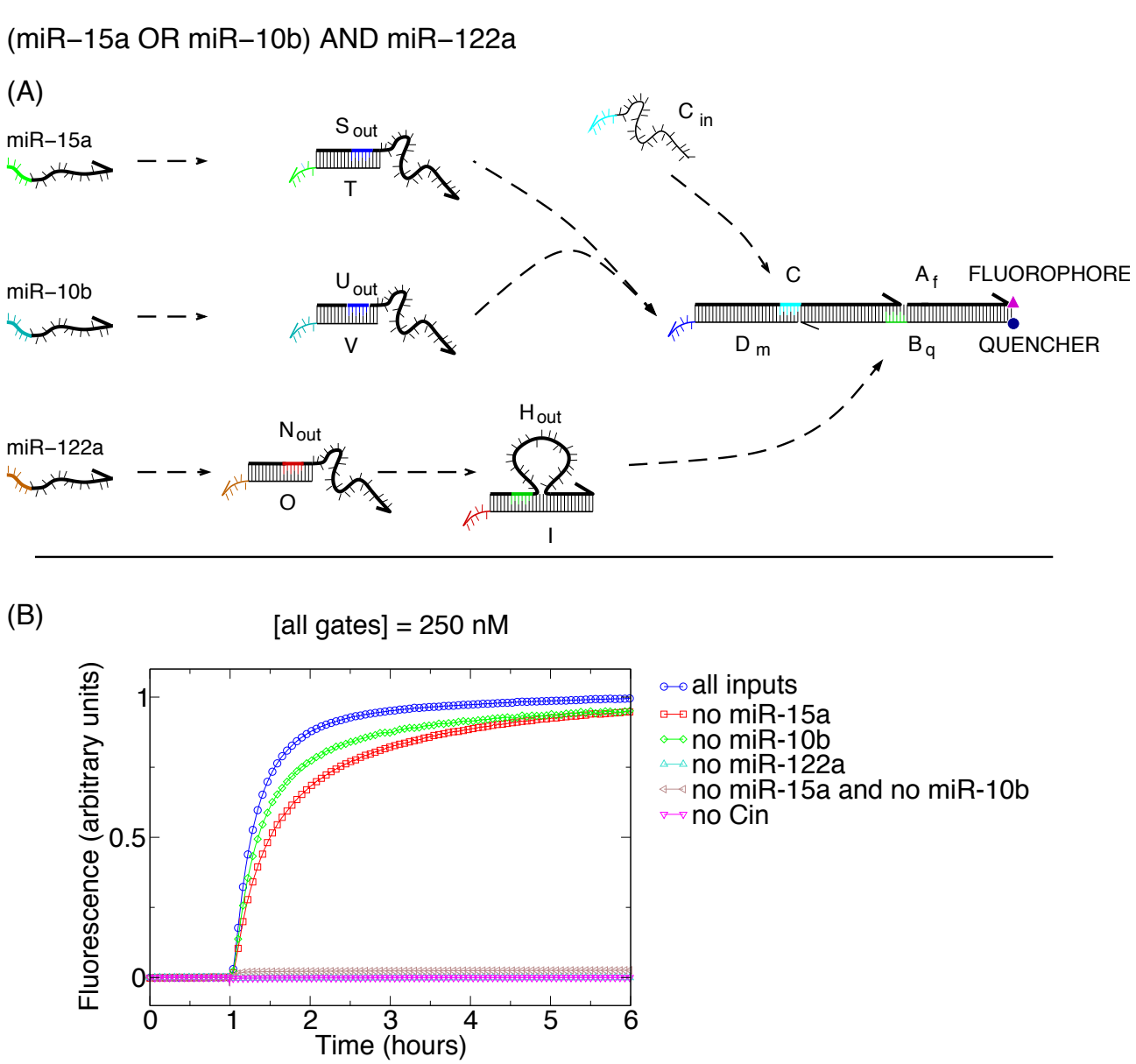

FIG. S8: Implicit OR and full translator. All gates are at 250 nM concentration and the inputs are at 300 nM. This circuit is an extended version of the implicit-OR circuit shown in Fig. S4B. Instead of adding input strand B_{in} directly as was done there, here miR-122a is used as an input and is translated into strand H_{out}. The recognition region of H_{out} has the same sequence as B_{in}. Note that the sequence of input H_{out} is completely unrelated to the sequence of miR-122a. If a single translator was used instead of the full translator (i.e. a cascade of two translators) this would not be true. In fact, strand N_{out} has six nucleotides in common with miR-122a.

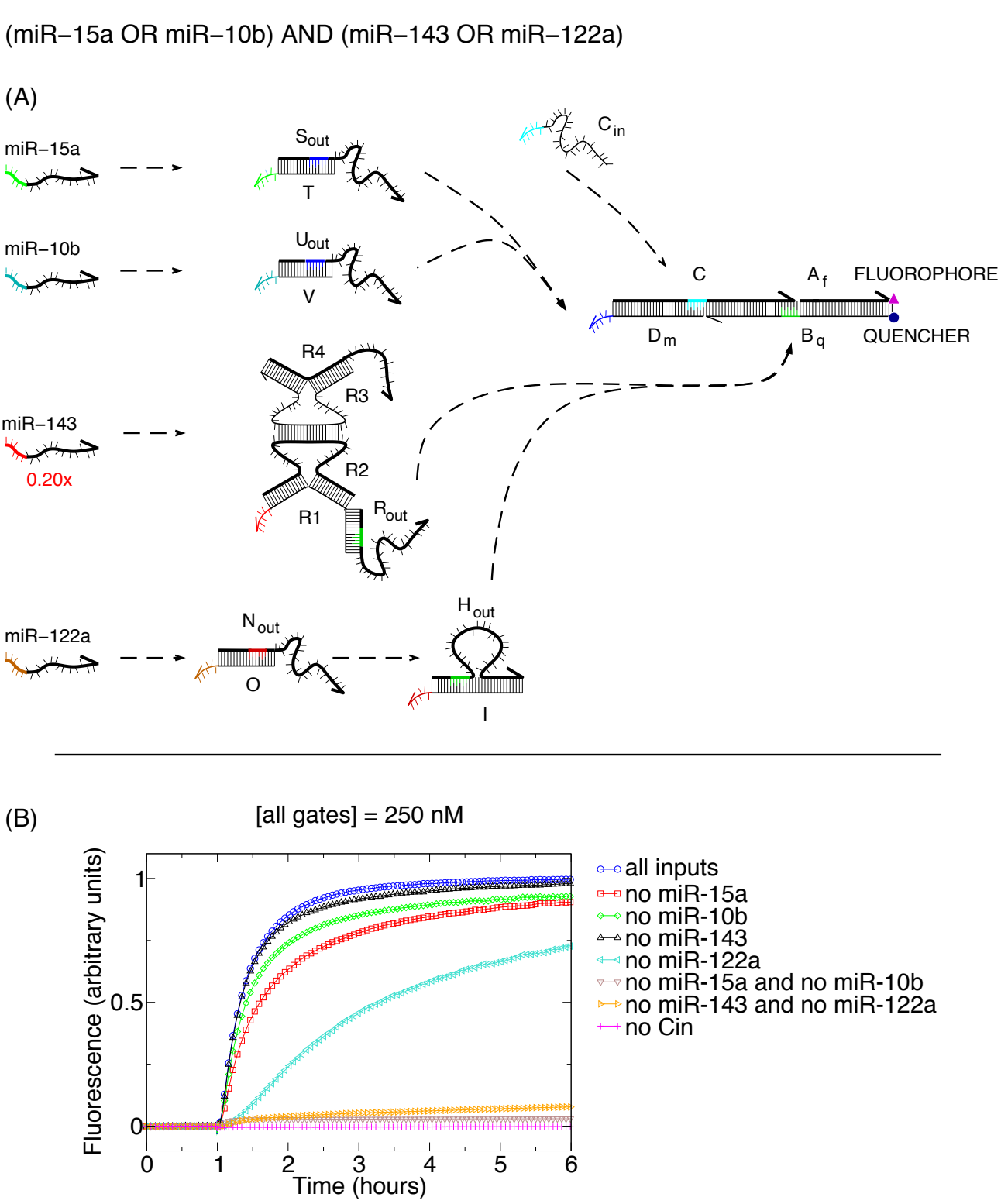

FIG. S9: Circuit with input amplifier. All gates at 250 nM, all inputs except miR-143 are at 300 nM (1.20x), while miR-143 is at 50 nM (0.20x). Note that miR-122a and miR-143 are coupled in an OR-clause. Only one of these two inputs thus is necessary for a logical TRUE output. In a situation where miR-122a is missing (and miR-143 is present) reaction kinetics are relatively slow since a substoichiometric amount of input needs to be catalytically amplified in order to fully trigger the fluorescently labeled three-input AND gate.

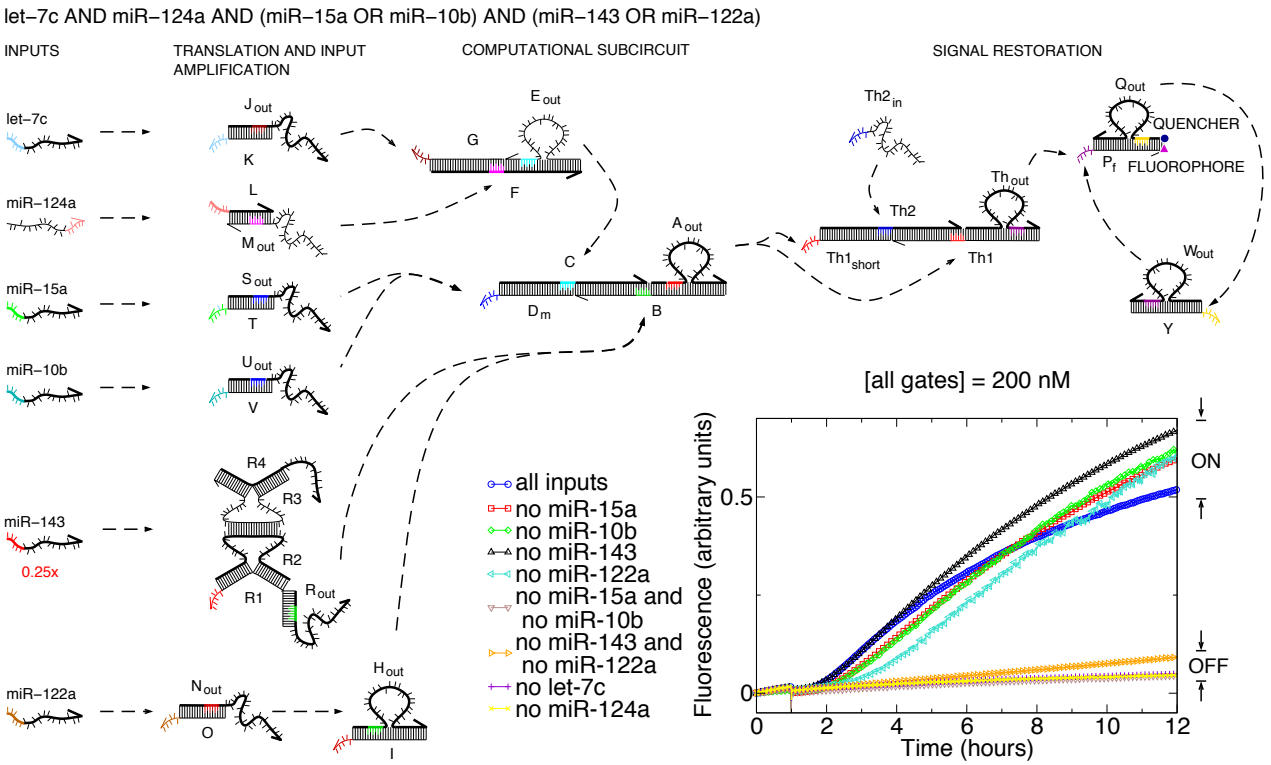

FIG. S10: Circuit with feedback-amplified output. All gates except threshold are at 200nM, the threshold gate is at 75 nM concentration. Input miR-143 is at 50 nM (0.25x) while all other inputs are at 250 nM (1.25x) concentration. With a total of 12 gates, this is the largest circuit we have constructed so far. We tested the case where all inputs are present (blue trace), all cases where exactly one input is missing (red, green, black, cyan, purple and yellow traces), and in addition, we tested withholding combinations of inputs constituting an OR clause (brown and orange traces). Assuming monotonicity, withholding additional inputs will never lead to a logical TRUE output. (Note that we did not test the simulated leaky miR-124a input in this series of experiments.)

TABLE S1: Gates, gate strands, inputs and outputs.

Gate	input 1	input 2	input 3	gate strands	output	ext. coeff.
$ABCD$	D_{in}	C_{in}, E_{out}	B_{in}, H_{out}	D, C, B	A_{out}	1847480
A_fB_qCD	D_{in}	C_{in}, E_{out}	B_{in}, H_{out}	D, C, B_q	A_f	1677057
$ABCD_m$	$D_{m,in}$, S_{out}, U_{out}	C_{in}, E_{out}	B_{in}, H_{out}, R_{out}	D_m, C, B	A_{out}	1869280
$A_fB_qCD_m$	$D_{m,in}$, S_{out}, U_{out}	C_{in}, E_{out}	B_{in}, H_{out}, R_{out}	D_m, C, B_q	A_f	1678177
EFG	J_{out}	M_{out}		G, F	E_{out}	1378540
E_qF_fG	J_{out}	M_{out}		G, F_f	E_q	1183277
$E_qF_fG_{not}$	$J_{out,not}$	M_{out}		G_{not}, F_f	E_q	1180697
JK	*let*-7*c*			K	J_{out}	622000
JK_{not}	K			*let*-7*c*3	$J_{out,not}$	598380
LM	*miR*-124*a*			L	M_{out}	624880
NO	*miR*-122*a*			O	N_{out}	669860
HI	N_{out}			I	H_{out}	851040
PQ	A_{out}, W_{out}			P	Q_{out}	907317
input amp.	*miR*-143			R_1, R_2, R_3, R_4	R_{out}	–
ST	*miR*-15*a*			T	S_{out}	625300
UV	*miR*-10*b*			V	U_{out}	619180
WY	Q_{out}			Y	W_{out}	825140
threshold	A_{out}	$Th2_{in}$	A_{out}	$Th1_{short}$, $Th2$, $Th1$,	Th_{out}	1874440
signal amp.	Th_{out}			$CA1$, $CA2$, $CA3$, $CA4$	–	–

TABLE S2: Input strand sequences. MicroRNA sequences are from Ref. [S7] and Ref. [S8]. All toe-holds and toe-hold binding regions are shown in gray, while recognition regions (including toe-holds) are underlined. Here, we omitted the terminal nucleotide from the concensus miR-122a sequence.

Strand	sequence
B_{in}	TTGGAGGTGTTTATAGCGGACCCCTACTGAGTTGTG
C_{in}	CTCCAAGAGTGATATGCCAATACAAACCACGAAGAC
D_{in}	CGGTTTCACATTACTTTTGCTGCCTTACGAGTCTTC
$D_{m,in}$	TTTGTGCACATTACTTTTGCTGCCTTACGAGTCTTC
D_{in}-*no-toe*	CACATTACTTTTGCTGCCTTACGAGTCTTC
F_{in}	GTTAGATGTTAGTTTCACGAAGACAATGATTAAGGC
G_{in}	TATGGTTGTTTATGTGTTCCCTGATCTTTAGCCTTA
G_{in}-*no-toe*	TGTTTATGTGTTCCCTGATCTTTAGCCTTA
let-7c	TGAGGTAGTAGGTTGTATGGT
let-7c-no-toe	AGTAGGTTGTATGGTTGT
miR-124a	TAAGGCACGCGGTGAATGCC
miR-124a-no-toe	GATTAAGGCACGCGGTG
miR-15a	TAGCAGCACATAATGGTTTGTG
miR-15a-no-toe	CACATAATGGTTTGTGCAC
miR-10b	CCCTGTAGAACCGAATTTGTGT
miR-10b-no-toe	AGAACCGAATTTGTGCAC
miR-122a	TGGAGTGTGACAATGGTGTTTG
miR-122a-no-toe	GTGACAATGGTGTTTGGAT
miR-143	TGAGATGAAGCACTGTAGCTCA
I_{in}-*no-toe*	GATGAATTGGAGGTGGGATATTATTACTGA
$Th2_{in}$	CGCTATCTGACTGACTGTTACCGATTTGTTTCATTC

TABLE S3: Gate and output strand sequences. Dye and quencher positions are indicated: TAM stands for TAMRA(NHS Ester) and IB_RQ for IowaBlack_RQ. All toe-holds and toe-hold binding regions are shown in gray and recognition regions (including toe-holds) are underlined.

Strand	sequence
A	GTGTTTATAGCGGACTGACGGTTTCACTACCCTGTTGTTCTACCCTACTGAGTTGTG
A_{out}	GTGTTTATAGCGGACTTACTAGATTTATACCCTGTTGAATGACCCTACTGAGTTGTG
A_f	GTGTTTATAGCGGACCCCTACTGAGTTGTG/TAM/
B	CACAACTCAGTAGGGGTCCGCTATAAACACCTCCAAGAGTGATATGCCAATACAAACCAC
B_q	/IB_RQ/CACAACTCAGTAGGGGTCCGCTATAAACACCTCCAAGAGTGATATGCCAATACAAACCAC
C	CACATTACTTTTGCTGCCTTACGAGTCTTCGTGGTTTGTATTGGCATATCACTCTTGGAG
D	GAAGACTCGTAAGGCAGCAAAAGTAATGTGAAACCG
D_m	GAAGACTCGTAAGGCAGCAAAAGTAATGTGCACAAA
E_{out}	GTTAGATGTTAGTTTCTCCAAGAGTGATATGCCAATACAAACCACGAAGACAATGAT
E_q	/IB_RQ/GTTAGATGTTAGTTTCACGAAGACAATGAT
F	TGTTTATGTGTTCCCTGATCTTTAGCCTTAATCATTGTCTTCGTGAAACTAACATCTAAC
F_f	TGTTTATGTGTTCCCTGATCTTTAGCCTTAATCATTGTCTTCGTGAAACTAACATCTAAC/TAM/
G	TAAGGCTAAAGATCAGGGAACACATAAACAACCATA
G_{not}	TAAGGCTAAAGATCAGGGAACACATAAACATGAGGT
H_{out}	GATGAATTGGAGGTGTTTATAGCGGACCCCTACTGAGTTGTGGGATATTATTACTGA
I	TCAGTAATAATATCCCACCTCCAATTCATCCAAACA
J_{out}	AGTAGGTTGTATGGTTGTTTATGTGTTCCCTGATCTTTAGCCTTA
$J_{out,not}$	CAACCTACTACCTCATGTTTATGTGTTCCCTGATCTTTAGCCTTA
K	ACAACCATACAACCTACTACCTCA
$let\text{-}7c3$	ACATGAGGTAGTAGGTTGTATGGT
L	GGCATTCACCGCGTGCCTTAATC
M_{out}	GTTAGATGTTAGTTTCACGAAGACAATGATTAAGGCACGCGGTG
N_{out}	GTGACAATGGTGTTTGGATGAATTGGAGGTGGGATATTATTACTGA
O	ATCCAAACACCATTGTCACACTCCA
P_f	AACAGGGTAACTCAGGAACAGGTCCGCTATGTCAGG/TAM/
Q_{out}	/IB_RQ/CCTGACATAGCGGACTGACGGTTTCACTACCCTGTTGTTCTACTGTTCCTGAGTTAC
R_1	CACCTCCAATTCATCAATGAGGGTGACTTCTGAGCTACAGTGCTTCATCTCA
R_2	GAAGCACTGTAGCTCACACACAGTAGATCAGAATTGGCACGTTCGCTCGCTAGGTTGAAGTCACCCTCATT
R_3	ATCAATGAGGGTGACTTCAACCTAGCGAGCGAACGTGCCAATTCTGATCTACTGTGTGTGAGCTACAGTGCTTCA
R_4	TGAAGCACTGTAGCTCAGAAGTCACCCTCATTGATGAATTGGAG
R_{out}	GATGAATTGGAGGTGTTTATAGCGGACCCCTACTGAGTTGTG
S_{out}	CACATAATGGTTTGTGCACATTACTTTTGCTGCCTTACGAGTCTTC
T	GTGCACAAACCATTATGTGCTGCTA
U_{out}	AGAACCGAATTTGTGCACATTACTTTTGCTGCCTTACGAGTCTTC
V	GTGCACAAATTCGGTTCTACAGGG
W_{out}	GACTGACGGTTTCACCCTGACATAGCGGACCTGTTCCTGAGTTACCCTGTTGTTCTA
Y	TAGAACAACAGGGTAGTGAAACCGTCAGTCCGCTAT
Th_{out}	GACTTACTAGATTTACCTGACATAGCGGACCTGTTCCTGAGTTACCCTGTTGAATGA
$Th1$	TCATTCAACAGGGTATAAATCTAGTAAGTCCGCTATCTGACTGACTGTTACCGATTTGTT
$Th2$	GACTTACTAGATTTATACCCTGTTGAATGAAACAAATCGGTAACAGTCAGTCAGATAGCG
$Th1_{short}$	TCATTCAACAGGGTATAAATCTAGTAAGTCCGCTAT
$CA2$	AACAGGGTAACTCAGGAACAGCACACAGTAGATCAGAATTGGCACGTTCGCTCGCTAGGTTGAAGTCACCCTCATT
$CA3$	/IB_RQ/AATGAGGGTGACTTCAACCTAGCGAGCGAACGTGCCAATTCTGATCTACTGTGTGCTGTTCCTGAGTTAC
$CA1$	AATGAGGGTGACTTCCTGTTCCTGAGTTAC
$CA4$	GTAACTCAGGAACAGGAAGTCACCCTCATT/TAM/

[S1] Puglisi, J. D. & Tinoco, I., Jr. (1989) in Methods in Enzymology **180**, eds. Dahlberg, J. E. & Abelson, J. N. (Academic Press, San Diego), 304–325.
[S2] Seelig, G., & Yurke, B., & Winfree, E. (2006) J. Am. Chem. Soc., **128**, 12211–12220.
[S3] Hofacker, I. & Fontana, W. & Stadler, P. & Bonhoeffer, L. & Tacker, M. & Schuster, P. (1994) Chemical Monthly **125**, 167–188.
[S4] SantaLucia, Jr., J. (1998) Proc. Natl. Acad. Sci. USA **95**, 1460–1465.
[S5] Seeman, N. C. (1982) J. Theor. Biol. **99**, 237–247.
[S6] Dirks, R. M., & Lin, M. & Winfree, E. & Pierce, N. A. (2004) Nucleic Acids Research **32**, 1392–1403.
[S7] Lagos-Quintana, M., & Rauhut, R., & Yalcin, A., & Meyer, J., & Lendeckel, W., & Tuschl, T. (2002) Current Biology **12**, 735–739.
[S8] Lagos-Quintana, M., & Rauhut, R., & Meyer, J., & Borkhardt, A., & Tuschl, T. (2003) RNA **9**, 175–179.